Organic/Inorganic Langmuir−Blodgett Films Based on Metal Phosphonates. 3. An Azobenzene-Derivatized Phosphonic Acid Forms Continuous Lattice Layers with Divalent, Trivalent, and Tetravalent Metal Ions[1]

Melissa A. Petruska and Daniel R. Talham*

Department of Chemistry, University of Florida, Gainesville, Florida 32611-7200

Received June 4, 1998. Revised Manuscript Received August 27, 1998

Metal phosphonate Langmuir−Blodgett (LB) films of an azobenzene-functionalized phosphonic acid amphiphile, (4-(4′-tetradecyloxyphenyldiazenyl)phenyl)butylphosphonic acid (**A4**), have been prepared with Zr^{4+}, La^{3+}, Gd^{3+}, Ba^{2+}, Mn^{2+}, and Cd^{2+}. Film formation and quality are characterized with optical spectroscopy, X-ray diffraction (XRD), X-ray photoelectron spectroscopy (XPS), and attenuated total reflectance Fourier transform infrared (ATR-FTIR) spectroscopy. The azobenzene chromophores are strongly H-aggregated in all of the metal phosphonate LB films. With divalent and trivalent ions, the in-plane metal phosphonate structure observed in the LB films is the same as that found in analogous solid-state layered phosphonates and depends on the identity of the metal ion. Films of **A4** with the lanthanide ions La^{3+} and Gd^{3+} form with stoichiometry $MH(O_3PR)_2$. When Ba^{2+} is incorporated into the films, the $M(HO_3PR)_2$ structure-type is adopted, while Mn^{2+} and Cd^{2+} give rise to films of **A4** with the stoichiometry $M(O_3PR)\cdot H_2O$. In each of these cases, the inorganic continuous lattice crystallizes in the hydrophilic portion of the film formed by the **A4** amphiphiles during deposition. Films incorporating Zr^{4+} were prepared with a previously described three-step procedure which exploits the strong oxophilicity of the Zr^{4+} ion. The films form with stoichiometry $Zr(O_3PR)_2$, the same as that observed in solid-state zirconium phosphonate materials. Film transfer is shown to be facile when the spacing of the inorganic network and the packing of the organic chromophores is commensurate, while a mismatch in these preferred spacings affects the deposition process. The results demonstrate that the metal phosphonate continuous inorganic network can be formed in LB films of amphiphiles other than alkylphosphonic acids, including those with larger organic groups.

Introduction

Traditionally, the Langmuir−Blodgett (LB) technique has been considered a method of generating well-organized thin films of organic molecules.[2−4] In this procedure, amphiphilic molecules are first organized at an air−water interface and then transferred onto a solid support that is passed through the film. Alternately dipping the substrate down and up through the air/water interface generates a bilayer, and multilayer films can be prepared in this way. We have recently demonstrated that inorganic continuous lattice structures can be incorporated into the hydrophilic regions of LB films by modeling the films after known organic/inorganic layered solids.[1,5−14] LB films of octadecylphosphonic acid (OPA) with a variety of divalent,[6,9,10] trivalent,[12] and tetravalent metals ions[5,8,14] have been prepared, and in each case, the inorganic continuous lattice of the solid-state materials is observed in the hydrophilic regions of the LB bilayers. The inorganic lattice adds substantial lattice energy to the films, greatly enhancing their stability. In addition, the inorganic network allows physical phenomena associated with the solid-state analogues to be incorporated into the films. As an example, we have recently prepared a magnetic LB film based on manganese octadecylphosphonate.[10]

* To whom correspondence should be addressed.

(1) Part 2: Petruska, M. A.; Fanucci, G. E.; Talham, D. R. *Thin Solid Films* **1998**, in press.
(2) Roberts, G. G. *Langmuir−Blodgett Films*; Plenum Press: New York, 1990.
(3) Ulman, A. *An Introduction to Ultrathin Organic Films: From Langmuir−Blodgett to Self-Assembly*; Academic Press: Boston, MA, 1991.
(4) Blodgett, K. B. *J. Am. Chem. Soc.* **1935**, *57*, 1007.
(5) Byrd, H.; Pike, J. K.; Talham, D. R. *Synth. Met.* **1995**, *71*, 1977−1980.
(6) Byrd, H.; Pike, J. K.; Talham, D. R. *J. Am. Chem. Soc.* **1994**, *116*, 7903−7904.
(7) Byrd, H.; Whipps, S.; Pike, J. K.; Ma, J.; Nagler, S. E.; Talham, D. R. *J. Am. Chem. Soc.* **1994**, *116*, 295−301.
(8) Byrd, H.; Pike, J. K.; Talham, D. R. *Chem. Mater.* **1993**, *5*, 709−715.
(9) Seip, C. T.; Byrd, H.; Talham, D. R. *Inorg. Chem.* **1996**, *35*, 3479−3483.
(10) Seip, C. T.; Granroth, G. E.; Meisel, M. W.; Talham, D. R. *J. Am. Chem. Soc.* **1997**, *119*, 7084−7094.
(11) Petruska, M. A.; Fanucci, G. E.; Talham, D. R. *Chem. Mater.* **1998**, *10*, 177−189.
(12) Fanucci, G. E.; Seip, C. T.; Petruska, M. A.; Ravaine, S.; Nixon, C. M.; Talham, D. R. *Thin Solid Films* **1998**, in press.
(13) Talham, D. R.; Seip, C. T.; Whipps, S.; Fanucci, G. E.; Petruska, M. A.; Byrd, H. *Comments Inorg. Chem.* **1997**, *19*, 133−151.
(14) Byrd, H.; Pike, J. K.; Showalter, M. L.; Whipps, S.; Talham, D. R. In *Interfacial Design and Chemical Sensing*; Mallouk, T. E., Harrison, D. J., Eds.; American Chemical Society: Washington, 1994; ACS Symposium Series 561, pp 49−59.

10.1021/cm980406z CCC: $15.00
Published on Web 10/22/1998

Layered metal phosphonates are known to form with different structural motifs, and several have now been observed in LB films. For example the lanthanide metals La^{3+}, Ce^{3+}, Sm^{3+}, and Gd^{3+} form with formula $MH(O_3PR)_2$ in both the LB films and solid-state materials.[15,16] The divalent metals Mn^{2+}, Cd^{2+}, Co^{2+}, and Mg^{2+} form with the stoichiometry $M(O_3PR)\cdot H_2O$ in the films and layered solids[17−20] while the structural motif in the Ba^{2+} octadecylphosphonate LB films is consistent with the layered solid-state analogues with formula $M(HO_3PR)_2$.[21] LB films modeled after layered zirconium phosphonates, $Zr(O_3PR)_2$,[22] have also been prepared although in this case, unlike in the divalent and trivalent metal phosphonate LB films, the inorganic layer is thought to be amorphous. By changing the metal ion, different metal phosphonate binding motifs are observed, and this in turn can lead to different arrangements of the organic groups in the LB films.

In traditional LB films, the organic groups are responsible for the properties of interest. However, with metal phosphonate-based LB films, the possibility of preparing mixed organic/inorganic assemblies where both the organic and inorganic components contribute to the function of the film now exists. While layered phosphonates have been formed from a variety of organophosphonic acids, metal phosphonate LB films have been primarily restricted to OPA. To explore the versatility of the metal phosphonate LB method, we wish to study LB films of functionalized organophosphonic acids to determine the limitations of forming the LB inorganic continuous lattice as the size and packing requirements of the organophosphonic acids change.

We report here on the preparation of metal phosphonate LB films based on the azobenzene-derivatized phosphonic acid ((4-((4′-tetradecyloxy)phenyl)diazenyl)-phenyl)butyl)phosphonic acid (**1**). We refer to this

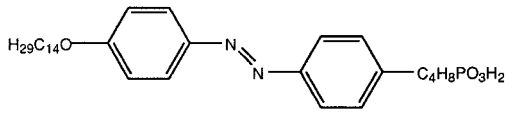

1

molecule as **A4**, where "**A**" indicates the azobenzene chromophore and "**4**" refers to the number of carbon atoms between the azobenzene moiety and the phosphonic acid headgroup. Azobenzenes have been widely studied in LB and self-assembled films with interests related to their optical properties,[23−25] nonlinear optical phenomena,[26−28] and the photochemically induced trans−cis isomerization reaction.[29−32] As a result, much is known about how azobenzene amphiphiles organize in LB films and how this organization can be probed with optical spectroscopy. We can therefore use the **A4** molecule to investigate how functional organic molecules organize in LB films that contain different metal phosphonate inorganic continuous lattice layers.

We describe LB films with several different metal ions. In each case the metal phosphonate continuous lattice structures are observed, demonstrating that the metal phosphonate LB approach can be used to form mixed organic/inorganic LB films containing functional organic groups. The preferred packing of the azobenzene chromophores is compared to the spacing requirements of the different metal phosphonate structure types. While for some structure types the ideal spacings of the organic and inorganic networks are similar, for others there is a significant mismatch. This difference in preferred spacings between the azobenzene chromophores and the metal phosphonate lattice affects the deposition process and suggests incommensurate organic and inorganic networks in the transferred films.

Experimental Section

Synthesis. *Materials.* Unless otherwise indicated, all reagents were purchased from either Aldrich (Milwaukee, WI) or Fisher Scientific (Pittsburgh, PA) and used as received. All reactions were performed under Ar or N_2 using glassware dried in an oven at 140 °C overnight unless otherwise specified. Dichloromethane was dried over P_2O_5 and freshly distilled prior to use. Triethyl phosphite was dried and distilled over Na. Triethylamine and pyridine were dried and distilled over CaH_2. 4-(4′-Hydroxybutyl)aniline (**2**) and 4-hydroxy-4′-(4″-hydroxybutyl)azobenzene (**3**) were prepared as previously described.[33]

Instrumentation. All NMR spectra were obtained on a Varian VXR-300 spectrometer. The characteristic solvent peaks were used as reference values (^1H, $CDCl_3$, 7.26 ppm; ^{13}C, $CDCl_3$, 77.0 ppm). Elemental analyses and mass spectrometry analyses were performed by the University of Florida Spectroscopic Services laboratory, where high-resolution mass spectra were collected on a MAT 95Q, Finnigan MAT (San Jose, CA). Melting points were obtained on a Thomas-Hoover Capillary melting point apparatus and are uncorrected. UV−vis spectra were obtained on a Hewlett-Packard 8452A diode array spectrophotometer. IR spectra as KBr pellets were recorded on a Mattson Instruments (Madison, WI) Research Series-1 FTIR spectrometer with a deuterated triglycine sulfate (DTGS) detector.

*4-Tetradecyloxy-4′-(4″-hydroxybutyl)azobenzene (**4**).* A mixture of **3** (3 g, 0.01 mol), bromotetradecane (3.3 mL, 0.01 mol),

(15) Cao, G.; Lynch, V. M.; Swinnea, J. S.; Mallouk, T. E. *Inorg. Chem.* **1990**, *29*, 2112−2117.
(16) Wang, R.-C.; Zhang, Y.; Hu, H.; Frausto, R. R.; Clearfield, A. *Chem. Mater.* **1992**, *4*, 864−870.
(17) Cao, G.; Lee, H.; Lynch, V. M.; Mallouk, T. E. *Solid State Ionics* **1988**, *26*, 63−69.
(18) Cao, G.; Lee, H.; Lynch, V. M.; Mallouk, T. E. *Inorg. Chem.* **1988**, *27*, 2781−2785.
(19) Frink, K. J.; Wang, R.; Colón, J. L.; Clearfield, A. *Inorg. Chem.* **1991**, *30*, 1438−1441.
(20) Cao, G.; Mallouk, T. E. *Inorg. Chem.* **1991**, *30*, 1434−1438.
(21) Poojary, D. M.; Zhang, B.; Cabeza, A.; Aranda, M. A. G.; Bruque, S.; Clearfield, A. *J. Mater. Chem.* **1996**, *6*, 639−644.
(22) Poojary, M. D.; Hu, H.; Campbell, I., F. L.; Clearfield, A. *Acta Crystallogr. B* **1993**, *49*, 996.
(23) Katayama, N.; Fukui, M.; Ozaki, Y.; Kuramoto, N.; Araki, T.; Iriyama, K. *Langmuir* **1991**, *7*, 2827−2832.
(24) Taniike, K.; Matsumoto, T.; Sato, T.; Ozaki, Y.; Nakashima, K.; Iriyama, K. *J. Phys. Chem.* **1996**, *100*, 15508−15516.
(25) Song, X.; Perlstein, J.; Whitten, D. G. *J. Am. Chem. Soc.* **1997**, *119*, 9144−9159.
(26) Katz, H. E.; Scheller, G.; Putvinski, T. M.; Schilling, M. L.; Wilson, W. L.; Chidsey, C. E. D. *Science* **1991**, *254*, 1485−1487.
(27) Eaglesham, A.; Jaworek, T.; Cresswell, J.; Allen, S.; Burgess, A.; Ferguson, I.; Ryan, T. G.; Hutchings, M.; Petty, M. C.; Yarwood, Y. *Langmuir* **1996**, *12*, 2292−2297.
(28) Lin, W.; Lin, W.; Wong, G. K.; Marks, T. J. *J. Am. Chem. Soc.* **1996**, *118*, 8034−8042.
(29) Liu, Z.-F.; Loo, B. H.; Baba, R.; Fujishima, A. *Chem. Lett.* **1990**, 1023−1026.
(30) Sato, T.; Ozaki, Y.; Iriyama, K. *Langmuir* **1994**, *10*, 2363−2369.
(31) Vélez, M.; Mukhopadhyay, S.; Muzikante, I.; Matisova, G.; Vieira, S. *Langmuir* **1997**, *13*, 870−872.
(32) Matsumoto, M.; Miyazaki, D.; Tanaka, M.; Azumi, R.; Manda, E.; Kondo, Y.; Yoshino, N.; Tachibana, H. *J. Am. Chem. Soc.* **1998**, *120*, 1479−1484.
(33) Jones, R.; Tredgold, R. H.; Hoorfar, A.; Allen, R. A.; Hodge, P. *Thin Solid Films* **1985**, *13*, 57−67.

and potassium carbonate (3 g, 2 equiv) in 80 mL of acetone was refluxed for 2 nights. At this time, 50 mL of diethyl ether and 50 mL of water were added, forming two layers. The organic layer was washed twice with 50 mL of a 2 M NaOH solution, once with 50 mL water, dried over Na_2SO_4, and concentrated in vacuo. Recrystallization of the residue from a diethyl ether/chloroform mixture produced the orange solid in 78% yield: mp 92−94 °C; ^{1}H NMR ($CDCl_3$) δ 7.89 (d, 2H), 7.80 (d, 2H), 7.30 (d, 2H), 6.99 (d, 2H), 4.03 (t, 2H), 3.67 (t, 2H), 2.71 (t, 2H), 1.79 (m, 2H), 1.74 (m, 2H), 1.61 (m, 2H), 1.46 (m, 2H), 1.40−1.20 (s, 20H), 0.88 (t, 3H); ^{13}C NMR ($CDCl_3$) δ 161.5, 151.1, 146.9, 145.0, 129.0, 124.5, 122.5, 114.6, 68.3, 62.7, 35.5, 32.2, 31.9, 29.6, 29.5, 29.4, 29.2, 27.4, 26.0, 22.7, 14.1.

*4-Tetradecyloxy-4′-(4″-bromobutyl)azobenzene (**5**).* A round-bottomed flask equipped with an addition funnel was charged with *p*-toluenesulfonyl chloride (0.11 g, 1.3 equiv) in 1 mL of pyridine and was placed in an ice/salt bath. To this was added **4** (0.2 g, 0.43 mmol) in 3 mL of pyridine dropwise from the addition funnel over 30 min. After stirring of the mixture in the ice bath for an additional 15 min, the round-bottomed flask was capped and placed in the refrigerator overnight. The next day the orange solution was added to a 13 mL ice/10 mL HCl solution causing solid to precipitate. The mixture was extracted twice with 50 mL of chloroform, once with 20 mL of a 50% ice/HCl solution, and twice with 50 mL of a saturated $NaHCO_3$ solution, dried over $MgSO_4$, and concentrated in vacuo. To this orange tosylated product was added LiBr (1.12 g, 0.013 mol) and 10 mL of acetone (dried and distilled over molecular sieves). The solution was refluxed overnight, at which time 50 mL of water was added. The product was extracted twice with 50 mL of diethyl ether, dried over $MgSO_4$, and concentrated in vacuo. Column chromatography of the residue on silica in a pentane/ether mobile phase eluted the product (R_f(2:1 pentane/diethyl ether) = 0.45) as an orange solid in 44% yield: mp 77−79 °C; ^{1}H NMR ($CDCl_3$) δ 7.90 (d, 2H), 7.81 (d, 2H), 7.30 (d, 2H), 7.00 (d, 2H), 4.03 (t, 2H), 3.43 (t, 2H), 2.71 (t, 2H), 1.89 (m, 2H), 1.82 (m, 4H), 1.47 (m, 2H), 1.40−1.20 (s, 20H), 0.88 (t, 3H); ^{13}C NMR ($CDCl_3$) δ 161.6, 151.3, 146.9, 144.5, 129.0, 124.6, 122.6, 114.7, 68.4, 34.8, 33.5, 32.2, 31.9, 29.7, 29.6, 29.4, 29.2, 26.0, 22.7, 14.1; HRMS (FAB) found *m*/*z* 529.2775, calcd for $C_{30}H_{46}N_2OBr$ *m*/*z* 529.2794 (M^+). Anal. Calcd for $C_{30}H_{45}N_2OBr$: C, 68.05; H, 8.51; N, 5.29. Found: C, 68.11; H, 8.72; N, 4.89.

*Diethyl (4-(4′-Tetradecyloxyphenyldiazenyl)phenyl)butylphosphonate (**6**).* Compound **5** (0.22 g, 0.42 mmol) was heated to 140 °C in a round-bottomed flask equipped with a distillation head and receiving flask. When the temperature stabilized, excess triethyl phosphite (0.25 mL, 3.5 eq) was added, and the formed EtBr was allowed to distill from solution. After the mixture was stirred overnight, the excess triethyl phosphite was removed. Column chromatography of the residue on silica in 100% diethyl ether eluted the starting material. Acetone/diethyl ether mixtures were used to elute the orange band (R_f(100% diethyl ether) = 0.21). Evaporation of this fraction gave the product as an orange/yellow solid in 74% yield: mp 53−55 °C; ^{1}H NMR ($CDCl_3$) δ 7.88 (d, 2H), 7.79 (d, 2H), 7.28 (d, 2H), 6.98 (d, 2H), 4.08 (m, 4H), 4.02 (t, 2H), 2.68 (t, 2H), 1.78 (m, 8H), 1.46 (m, 2H), 1.30 (t, 6H), 1.38−1.19 (s, 20H), 0.87 (t, 3H); ^{13}C NMR ($CDCl_3$) δ 161.5, 151.1, 146.9, 144.6, 129.0, 124.5, 122.6, 114.6, 68.3, 61.5, 61.4, 35.2, 32.2, 32.0, 31.9, 29.6, 29.5, 29.3, 29.2, 26.5, 26.0, 24.6, 22.6, 22.1, 22.0, 16.4, 14.1; HRMS (FAB) found *m*/*z* 587.3966, calcd for $C_{34}H_{56}N_2O_4P$ *m*/*z* 587.3978 (M^+).

*(4-(4′-Tetradecyloxyphenyldiazenyl)phenyl)butylphosphonic Acid (**1**).* To a solution of **6** (0.2 g, 0.34 mmol) in 12 mL of dichloromethane was added triethylamine (0.19 mL, 4 equiv) and bromotrimethylsilane (0.18 mL, 4 equiv). After being stirred for 6 h, the solution was concentrated in vacuo and 12 mL of methanol was added to the residue. Stirring was continued for 15 h when the orange precipitate was collected and washed with water, diethyl ether, and dichloromethane, giving the product in 72% yield: mp 185−186 °C; ^{1}H NMR ($CDCl_3$/CD_3CD_2OD) δ 7.70 (d, 2H), 7.60 (d, 2H), 7.12 (d, 2H), 6.82 (d, 2H), 3.87 (t, 2H), 2.52 (t, 2H), 1.58 (m, 8H), 1.30 (m, 2H), 1.20−1.10 (s, 20H), 0.69 (t, 3H); IR (KBr, cm^{-1}) 3450 (br), 2955, 2918, 2872 (sh), 2850, 2340 (br), 1602, 1586, 1501, 1474, 1395, 1298, 1248, 1154, 1107, 1040, 1029, 997, 941, 843, 721, 642, 538; UV λ_{max} ($CHCl_3$/CH_3CH_2OH) 246 nm (ϵ = 10 000 M^{-1} cm^{-1}), 354 nm (ϵ = 18 000 M^{-1} cm^{-1}), 442 nm (ϵ = 2000 M^{-1} cm^{-1}); HRMS (FAB) found *m*/*z* 531.3319, calcd for $C_{30}H_{48}N_2O_4P$ *m*/*z* 531.3352 (M^+). Anal. Calcd for $C_{30}H_{47}N_2O_4P$: C, 67.92; H, 8.87; N, 5.28. Found: C, 67.60; H, 9.09; N, 5.21.

Films. *Materials.* Unless otherwise noted, all reagents were used as received. Octadecylphosphonic acid (OPA), $C_{18}H_{39}O_3P$, was obtained from Alfa Aesar (Ward Hill, MA). Zirconyl chloride, 98%, and octadecyltrichlorosilane (OTS), $C_{18}H_{37}SiCl_3$, 95%, were purchased from Aldrich. HPLC grade chloroform, stabilized with amylene, was obtained from Acros (Pittsburgh, PA).

Substrate Preparation. Single-crystal (100) silicon wafers, purchased from Semiconductor Processing Co. (Boston, MA), were used as deposition substrates for X-ray photoelectron spectroscopy (XPS). X-ray diffraction samples were prepared on petrographic slides that were purchased from Buehler Ltd (Lake Bluff, IL). Silicon and germanium attenuated total reflectance (ATR) crystals, 50 mm × 10 mm × 3 mm with 45° faces, purchased from Wilmad Glass (Buena, NJ), were used as substrates for FTIR-ATR experiments. Quartz microscope slides (25 mm × 25 mm × 1 mm) were purchased from Chemglass (Vineland, NJ) and used as substrates for optical studies. The silicon, glass, and quartz substrates were cleaned using the RCA procedure[34] and dried under nitrogen. All substrate surfaces were made hydrophobic by deposition of a monolayer of OTS.[35,36]

Instrumentation. The Langmuir−Blodgett (LB) experiments were performed with a KSV Instruments (Stratford, CT) 5000 system with homemade Teflon-coated troughs modified to operate with double barriers. Pressure versus area (π−*A*) isotherms were recorded on this system with a trough surface area of 794 cm^2 (12.8 cm × 67 cm). A Barnstead NANOpure (Boston, MA) purification system produced water with a resistivity of 17.5−18 MΩ cm for all experiments. Surface pressure was measured with a platinum Wilhelmy plate suspended from a KSV microbalance. The pH of the subphase was adjusted with the appropriate amount of 0.012 M HCl or 0.01 M KOH (unless otherwise noted) and was stable over the time scale of the experiments. Elevated temperatures for the subphase were achieved with a constant-temperature circulator model 900 purchased from Fisher Scientific.

Infrared spectra were recorded on a Mattson Instruments (Madison, WI) Research Series-1 FTIR spectrometer with a deuterated triglycine sulfate (DTGS) detector. LB films were deposited onto OTS-coated Si or Ge ATR parallelograms, and a Harrick (Ossing, NY) TMP stage was used for the ATR experiments. Polarized FTIR-ATR spectra were taken with s- and p-polarized light. All FTIR-ATR spectra consist of 1000 scans at 4 cm^{-1} resolution and were referenced to the appropriate background.

X-ray diffraction patterns were obtained with a Phillips APD 3720 X-ray powder diffractometer with the Cu Kα line, λ = 1.54 Å as the source. XPS was performed on a Perkin-Elmer (Eden Prairie, MN) PHI 5000 series spectrometer. All spectra were taken using the Mg Kα line at 1253.6 eV. The spectrometer has a typical resolution of 2.0 eV, with anode voltage and power settings of 15 kV and 300 W, respectively. Typical operating pressure was 5 × 10^{-9} atm. All XPS spectra were recorded with a 45° takeoff angle. Survey scans consisted of 5 scans performed with 0.5 eV/step, 20 ms/step, and a pass energy of 89.45 eV, and multiplex scans consisted of 80 scans per region taken in 10 sweeps/cycle operating at 0.1 eV/step, 50 ms/step, and a pass energy of 37.75 eV.

(34) Kern, W. *J. Electrochem. Soc.* **1990**, *137*, 1887−1892.
(35) Maoz, R.; Sagiv, J. *J. Colloid Interface Sci.* **1984**, *100*, 465−496.
(36) Netzer, L.; Sagiv, J. *J. Am. Chem. Soc.* **1983**, *105*, 674−676.

Scheme 1. Synthesis of A4

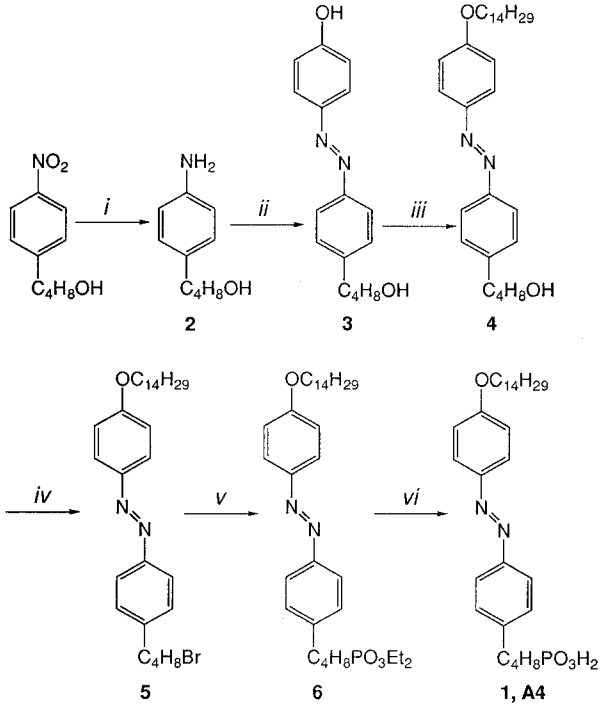

(*i*) Sn/HCl (*ii*) $NaNO_2$/HCl, phenol, NaOH (*iii*) $C_{14}H_{29}Br$, K_2CO_3
(*iv*) *p*-toluenesulphonyl chloride, LiBr (*v*) $P(OCH_2CH_3)_3$
(*vi*) $BrSi(CH_3)_3$, $N(CH_2CH_3)_3$, MeOH

UV–vis spectra were obtained with a Hewlett-Packard 8452A diode array spectrophotometer. Photolysis experiments were performed with a 450 W Hanovia lamp. A LG350 filter and a Corning 7-54 filter were used to isolate the 365 nm mercury line for the trans to cis isomerization. Photochemical isomerization of *cis*-azobenzene was accomplished with the use of a LG 450 filter, which blocked light of wavelengths shorter than 440 nm.

Results

Synthesis and Characterization of A4. The synthetic steps used to prepare **A4**, shown in Scheme 1, are well-documented procedures.[33,37–40] After the synthesis of the azobenzene unit, bromination of the alcohol and the subsequent Arbuzov reaction[37] afford the phosphonate ester of **A4** which is conveniently dealkylated with bromotrimethylsilane and hydrolyzed with methanol[40] to yield the analytically pure **A4**.

The photochemistry of azobenzene and its derivatives is well-established.[41–44] The trans form of azobenzene, the more stable of the two isomers, is characterized by a $\pi-\pi^*$ transition in the UV region and a weak, symmetry-forbidden $n-\pi^*$ transition near 450 nm that accounts for the yellow color of the azobenzene solid. Irradiation of *trans*-azobenzene at 365 nm produces rotation about the N–N double bond to form the cis isomer. On conversion to the cis form, the $\pi-\pi^*$ transition shifts to shorter wavelengths, and the band corresponding to the $n-\pi^*$ transition, which is symmetry allowed in the cis isomer, becomes more intense. The cis isomer is normally short-lived, and conversion back to trans azobenzene can be effected thermally or photochemically (with light of wavelength greater than 440 nm). Compound **A4** behaves like many azobenzene derivatives. In a chloroform/ethanol solution its $\pi-\pi^*$ transition is found at 354 nm ($\epsilon = 18\,000\ M^{-1}\,cm^{-1}$), as seen in Figure 1, a value typical for a nonaggregated azobenzene chromophore substituted in a similar manner.[41,45] Upon irradiation, as **A4** is converted to its cis isomer, the $\pi-\pi^*$ transition shifts to 310 nm and the $n-\pi^*$ transition at 442 nm increases in intensity (Figure 1). The isomerization is nearly quantitative for **A4** in solution. This process is reversible, and after 3 h the short-lived cis isomer has almost completely reverted back to the trans form.

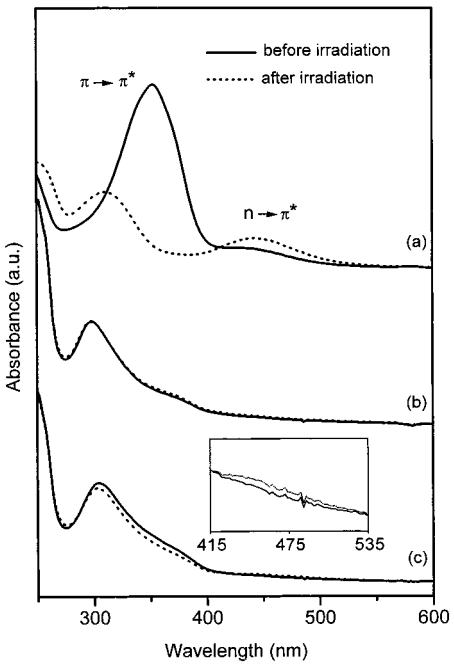

Figure 1. Optical spectra before and after irradiation at 365 nm of (a) **A4** in a chloroform/ethanol solution, (b) five bilayers of an **A4**/La/**A4** film, and (c) five bilayers of an **A4**/Zr/**A4** film. The inset in (c) shows the increase in the characteristic cis $n-\pi^*$ transition after irradiation at 365 nm. Band assignments are discussed in the text.

Deposition Procedures. Bilayers of **A4** with divalent and trivalent metals are transferred onto hydrophobic supports using conventional vertical dipping methods.[2] In each case the deposition conditions are important considerations. In particular, the pH of the subphase plays a crucial role in film formation.[10,12] If the pH of the subphase is too low, films transfer with incomplete metal binding. On the other hand, if the pH is too high, the metal ions cross-link with the phosphonate groups on the water surface, making the films too rigid to transfer. During the deposition procedure, a

(37) Bhattacharya, A. K.; Thyagarajan, G. *Chem. Rev.* **1981**, *81*, 415–430.
(38) Katz, H. E.; Wilson, W. L.; Scheller, G. *J. Am. Chem. Soc.* **1994**, *116*, 6636–6640.
(39) Katz, H. E.; Bent, S. F.; Wilson, W. L.; Schilling, M. L.; Ungashe, S. B. *J. Am. Chem. Soc.* **1994**, *116*, 6631–6635.
(40) McKenna, C. E.; Higa, M. T.; Cheung, N. H.; McKenna, M.-C. *Tetrahedron Lett.* **1977**, 155–158.
(41) Ross, D. L.; Blanc, J. In *Photochromism*; Brown, G. H., Ed.; John Wiley and Sons: New York, 1971; Vol. 3, pp 471–556.
(42) Griffiths, J. *Chem. Soc. Rev.* **1972**, *1*, 481–493.
(43) Rau, H. In *Photochemistry and Photophysics*; Rabek, J. F., Ed.; CRC Press: Boca Raton, FL, 1990; Vol. 2, pp 119–141.
(44) Wyman, G. M. *Chem. Rev.* **1955**, *55*, 625–657.
(45) Shimomura, M.; Ando, R.; Kunitake, T. *Ber. Bunsen-Ges. Phys. Chem.* **1983**, *87*, 1134–1143.

Table 1. Deposition Conditions[a] for the A4 LB Monolayers and Bilayers

	target pressure (mN/m)	dipping speeds[b] (mm/min)	pH range
	Monolayers (Zr)		
template	35	3	NA[c]
capping	35	2	NA[c]
	Bilayers		
La	28	5; 3	2.2−2.4
Gd	32−33	5; 3	1.2−1.3
Ba	20−22	5; 3	8.4−8.8
Mn[d]	24−27	5; 3	3.9−4.2

[a] For all depositions, films were compressed with a linear compression rate of 8 mN/(m/min) and with barrier speeds of 20−30 mm/min. [b] For bilayers with 2 speeds indicated, the first number corresponds to the speed of the dipper on the downstroke while the second number is for the upstroke. [c] pH was not adjusted for these films. [d] The subphase temperature was 41 °C for Mn^{2+}; all other films were deposited at room temperature.

Langmuir monolayer is compressed to the desired target pressure and an octadecyltrichlorosilane (OTS)-coated substrate is dipped down into the well of the trough, filled with a 0.5 mM solution of the metal ion, to transfer a monolayer oriented with the alkyl tails of the amphiphiles toward the hydrophobic substrate. As the substrate is withdrawn from the trough, a second layer is transferred to form a head-to-head bilayer, and if the pH is adjusted appropriately, the metal phosphonate continuous lattice crystallizes as the water drains from the film.[10,12] The transfer conditions for each metal examined are found in Table 1. The transfer ratios, after correction for the creep of the **A4** film, are 1.0 ± 0.1 unless otherwise noted.

Unlike the divalent and trivalent metal phosphonate films, the tetravalent Zr^{4+} phosphonates cannot be transferred with conventional vertical dipping methods. Previous work with metal phosphonate LB films has shown that the strong oxophilicity of the zirconium ion precludes transfer of the phosphonate films when zirconium ions are present in the subphase because of the substantial cross-linking of the metal ions and phosphonate groups on the water surface.[1,7,8,11] However, zirconium phosphonate LB films can be deposited using a three-step deposition procedure,[7,8] and this method was used to deposit **A4** films with Zr^{4+}. As illustrated in Scheme 2, the first step involves creation of an LB monolayer by dipping an OTS-coated substrate down through a compressed monolayer on a pure water subphase into a vial sitting in the dipping well of the trough. We refer to this layer deposited on the downstroke as the "template" layer. The Langmuir monolayer is then decompressed, and the vial containing the template-coated substrate is removed from the trough. In the second step, an aqueous solution of $ZrOCl_2$ is added to the vial to bind Zr^{4+} ions to the template. After 20 min the substrate containing the zirconated template layer is removed from the solution, rinsed with water, and returned to the trough. The zirconated template is stable, and information about its organization and structure can be obtained. For the final step, a new Langmuir monolayer is compressed at the air−water interface, and a new LB monolayer is deposited as the substrate is drawn upward through the film. The layer deposited onto the zirconated template is referred to as the "capping" layer. Multilayer assemblies are prepared by repeating this three-step procedure. Transfer ratios

Scheme 2. Three-Step Procedure for the Deposition of Zirconium Phosphonate Bilayers

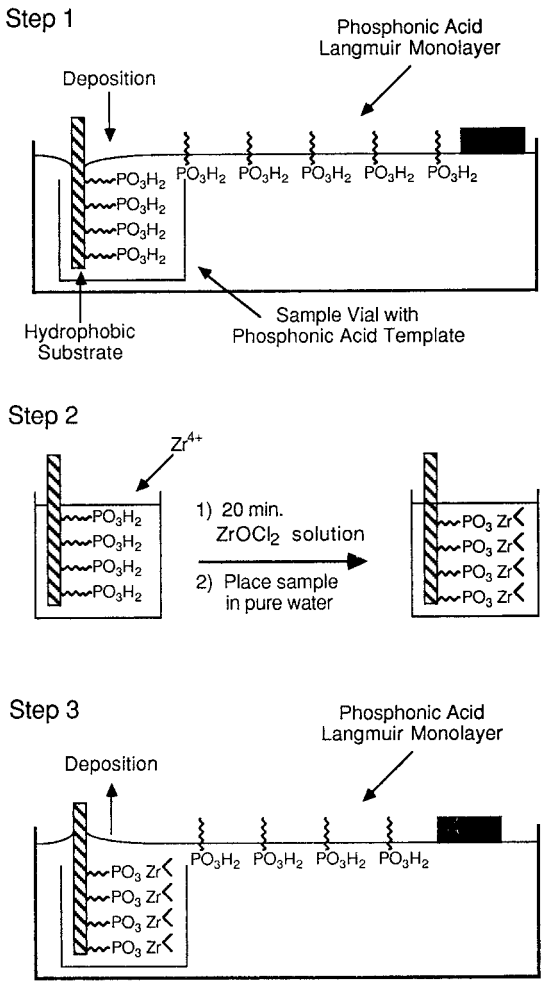

were 1.0 ± 0.1 after correction for creep of the **A4** film. The deposition conditions used to prepare the zirconium phosphonate films are also listed in Table 1.

Characterization of Metal Phosphonate LB Films. The metal ions studied form different metal phosphonate structure types in the solid state, and this was also observed in the **A4** LB films. Films deposited with La^{3+} and Gd^{3+} form the $MH(O_3PR)_2$ phase, Ba^{2+} forms with formula $M(HO_3PR)_2$, and Mn^{2+} and Cd^{2+} form the $M(O_3PR)\cdot H_2O$ phase. The Zr^{4+} films possess an amorphous inorganic layer but are consistent with the $Zr(O_3PR)_2$ stoichiometry. Below, we have organized the characterization of the **A4** films according to the observed metal phosphonate structure type. The lanthanide phosphonate films are described in detail to illustrate what each of the characterization methods can tell us about film structure.

Films with Structure Type $MH(O_3PR)_2$. In the optical spectrum of five bilayers of an **A4** lanthanum phosphonate film, Figure 2, the $\pi-\pi^*$ transition observed at 354 nm in a chloroform/ethanol solution is blue-shifted to 298 nm. According to the molecular exciton model,[46] this shift to higher energy indicates that the azobenzene units pack as H-aggregates, with a parallel alignment

(46) McRae, E. G.; Kasha, M. In *Physical Processes in Radiation Biology*; Augenstein, L., Mason, R., Rosenberg, B., Eds.; Academic Press: New York, 1964; pp 23−42.

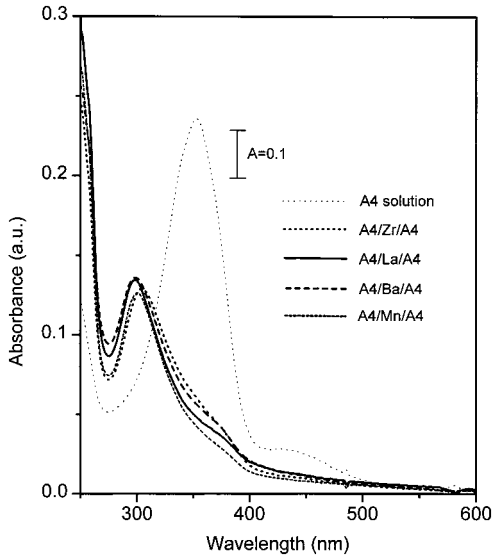

Figure 2. Room-temperature optical spectra of five bilayer metal phosphonate LB films of **A4** with zirconium, lanthanum, barium, and manganese. The solution spectrum of **A4** (chloroform/ethanol) is included for comparison. The absorbance scale at the left refers to the LB films. The blue shift of the $\pi-\pi^*$ band to near 300 nm indicates H-aggregation of the azobenzene chromophores in the LB films.

of the chromophores within the films. For H-aggregates, the transition allowed exciton state of the aggregate is at a higher energy than the allowed excited state of the monomer, thereby accounting for the observed hypsochromic shift. From the magnitude of this shift (56 nm) it is likely that there is long-range organization in the azobenzene packing.[25] A second $\pi-\pi^*$ band is observed at 250 nm. The relative intensities of the two $\pi-\pi^*$ bands change from the solution spectrum to the LB film spectrum. The 250 nm band has its transition moment perpendicular to the long axis of the chromophore while the transition moment of the lower energy band is parallel to the azobenzene long axis. The stronger intensity of the 250 nm band, relative to the 298 nm peak in the transferred films, indicates that the long axes of the chromophores are oriented nearly perpendicular to the substrate.[30] A slight shoulder on the low-energy side of the 298 nm band is at the same energy as the $\pi-\pi^*$ transition of **A4** in the solution spectrum. It is likely that there are a few areas in the films in which the azobenzene units are present as monomers or dimers, which do not exhibit a blue shift in the transition.[25]

Irradiation of the $\pi-\pi^*$ transition with UV light induces an inefficient trans–cis isomerization of the azobenzene chromophores, and this is evidenced in Figure 1 where no change in the optical spectrum is observed during the irradiation. After irradiation at 365 nm, we see no evidence for the $n-\pi^*$ transition that characterizes the cis isomer. It is probable that some chromophores still undergo isomerization in the defect areas and domain boundaries in the films where there is a higher concentration of isolated chromophores and dimers.[31] However, the inefficient trans–cis isomerization suggests that organized domains are well-defined in the trivalent phosphonate films.

X-ray photoelectron spectroscopy (XPS) survey scans reveal that the elements present in the films are C, N, O, P, and either La or Gd. Analysis of the integrated areas in XPS multiplex scans affords the relative ratios of phosphorus to metal atoms in the films.[47–51] Corrections are applied to account for differences in photoelectron escape depths and the layered geometry of the film, and the results are listed in Table 2. In the **A4**/La/**A4** film the predicted ratios[52] are in agreement, within experimental error (±5%), with the 2:1 P:La ratio present in the lanthanum organophosphonate solid-state materials. Such an analysis was not performed in the case of the **A4**/Gd/**A4** film because the peaks arising from the Gd atoms in the survey scan overlap signals from other atoms.

Bragg peaks observed for each sample in X-ray diffraction (XRD) measurements confirm the layered nature of the films. XRD from 10 bilayers of the lanthanide films yielded patterns with 8 (00*l*) reflections in each case. The pattern for the **A4**/La/**A4** film is seen in Figure 3. The intensity of the diffraction patterns is very strong for these films relative to other metal phosphonate LB films,[10] reflecting the large electron density of the lanthanide ions. Interlayer spacings of 67 Å (±2 Å) (Table 2) for each of the lanthanide phosphonate films reflect the presence of the azobenzene chromophore in the films.

Table 2. Interlayer Spacings[a] Measured from XRD and Relative Intensities[b] of the Metal and Phosphorus[c] XPS Signals of the LB Monolayer and Bilayer Films

	XPS peak	obsd rel intensity (±5%)	calcd rel intensity[d]	*d*-spacing (±2 Å)
	Zirconated Template			
A4/Zr	Zr_{3d} (186.4, 184.2 eV)	53	50	NA
	P_{2p}	47	50	
	Bilayer Samples			
A4/Zr/A4	Zr_{3d} (186.4, 184.2 eV)	32	33	63
	P_{2p}	68	67	
A4/La/A4	La_{3d} (836.4 eV)	8	8	67
	P_{2p}	92	92	
A4/Gd/A4	Gd_{4d} (143.8 eV)	NA[e]	NA[e]	67
	P_{2p}			
A4/Ba/A4	Ba_{3d} (796.5 eV)	19	20	66
	P_{2p}	81	80	
A4/Mn/A4[f]	Mn_{2p} (654.5, 643.1 eV)	25	28	64
	P_{2p}	75	72	

[a] X-ray samples consisted of 10 bilayers of deposited films. [b] Relative intensities are reported as the percentage of the sum of the integrated areas of the metal and phosphorus peaks after correcting for elemental sensitivity factors. [c] Binding energy of P_{2p} is 134.5 eV for all samples. [d] Assuming a layered structure, using a model described in ref 52. The observed photoelectron intensities are attenuated by the **A4** layer. Relative intensities of the phosphorus and metal ions in the films were calculated using the inelastic mean free path values $\lambda_{Zr} = 23.4$ Å, $\lambda_{La} = 6.3$ Å, $\lambda_{Ba} = 15.3$ Å, $\lambda_{Mn} = 7.7$ Å, $\lambda_P = 23.9$ Å for the zirconium and barium films, and $\lambda_P = 10.4$ Å for the lanthanum and manganese films. [e] Relative intensities are inconclusive due to the presence of overlapping peaks. [f] This film is prepared from a subphase heated to 41 °C.

(47) Brundle, C. R.; Hopster, H.; Swalen, J. D. *J. Chem. Phys.* **1979**, *70*, 5190–5196.
(48) Seah, M. P.; Dench, W. A. *Surf. Interface Anal.* **1979**, *1*, 1–11.
(49) Akhter, S.; Lee, H.; Hong, H.-G.; Mallouk, T. E.; White, J. M. *J. Vac. Sci. Technol.* **1989**, *7*, 1608–1613.
(50) Laibinis, P. E.; Bain, C. D.; Whitesides, G. M. *J. Phys. Chem.* **1991**, *95*, 7017–7021.
(51) Sastry, M.; Ganguly, P.; Badrinarayanan, S.; Mandale, A. B.; Sainkar, S. R.; Paranjape, D. V.; Patil, K. R.; Chaudhary, S. K. *J. Chem. Phys.* **1991**, *95*, 8631–8635.
(52) Pike, J. K.; Byrd, H.; Morrone, A. A.; Talham, D. R. *Chem. Mater.* **1994**, *6*, 1757–1765.

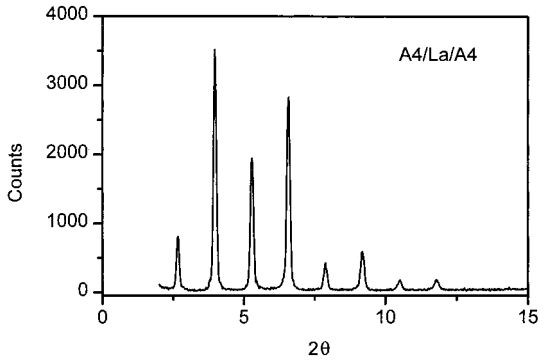

Figure 3. X-ray diffraction pattern from 10 bilayers of an **A4**/La/**A4** film. The layered nature of the film is confirmed by the 8 (00*l*) Bragg peaks observed.

While XPS and XRD studies confirm the stoichiometry and layered nature of the films, attenuated total reflectance Fourier transform infrared (ATR-FTIR) spectroscopy provides additional information about the in-plane organization of the transferred LB films.[10−12,35,53,54] The C−H stretches are found in the region between 3100 and 2700 cm^{-1}, and their position and full width at half-maximum (fwhm) reflect the extent of organization in the alkyl chains. More specifically, the frequency of the asymmetric methylene stretch ($\nu_a(CH_2)$) is sensitive to conformation[35,53] while its fwhm is influenced by the degree to which the alkyl chains are close-packed.[35,54] In the ATR-FTIR spectrum of the **A4** lanthanum phosphonate bilayer, the peak positions of the three characteristic C−H stretches, the asymmetric methyl stretch ($\nu_a(CH_3)$), $\nu_a(CH_2)$, and the symmetric methylene stretch ($\nu_s(CH_2)$), are observed at 2955, 2918, and 2850 cm^{-1}, respectively. The peak position of $\nu_a(CH_2)$ indicates that at least part of the alkyl chain segments is in an all-trans conformation.[55] The fwhm of $\nu_a(CH_2)$ is large in this film, and the broadening arises from the shoulder on this peak, as can be seen in Figure 4. The C−H stretches in the IR contain contributions from both the 4-carbon and 14-carbon segments of the **A4** amphiphile, and it is the 4-carbon chain which causes broadening of the 2918 cm^{-1} peak. This observation is consistent with results from a previous study of zirconium phosphonate LB films of phenoxy- and biphenoxy-derivatized amphiphiles substituted in a similar manner as **A4**.[11] After deuteration of the 14-carbon chains in those molecules, IR analysis revealed that the 14-carbon chains are close-packed and in an all-trans conformation while the 4-carbon segments in the films are not well-ordered. As with the phenoxy and biphenoxy examples, the IR bands suggest that the 14-carbon segments in this film are close-packed and in an all-trans conformation while the 4-carbon tethers are not well-ordered.

IR spectroscopy can also be used to compare the mode of metal phosphonate binding in the LB films to that of the analogous layered solid-state materials. The phosphonate P−O stretching bands are very sensitive to the mode of metal−phosphonate bonding and to the identity

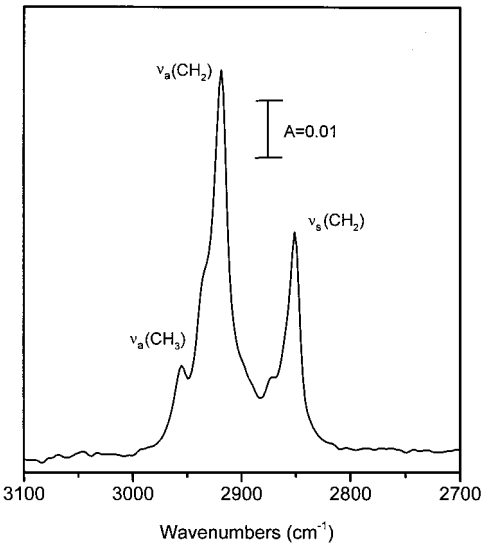

Figure 4. ATR-FTIR spectrum showing the carbon−hydrogen stretching modes of two bilayers of an **A4**/La/**A4** film. The shoulder (near 2935 cm^{-1}) on the high-energy side of the $\nu_a(CH_2)$ band is attributed to disorder in the four-carbon segment of **A4** in the film. Band assignments are discussed in the text.

of the metal ion.[18,56] Previous studies on OPA LB films with a similar series of divalent and trivalent metal ions have demonstrated that the structure of the metal phosphonate lattice in the LB films can be identified by comparing the P−O stretching bands in the LB film to those of the solid-state analogues.[10,12] The IR spectrum between 900 and 1800 cm^{-1} of the **A4**/La/**A4** film is seen in Figure 5B, along with a KBr spectrum of lanthanum butylphosphonate added to help identify the P−O bands. The asymmetric and symmetric P−O stretches appear in the region between 1160 and 960 cm^{-1}. These stretches are also present for the **A4**/La/**A4** film although they are slightly obscured by bands arising from the azobenzene chromophore (Figure 5A). Although the spectrum is complicated by the presence of overlapping signals of **A4**, the significant P−O stretch at 1107 cm^{-1} is at the same frequency in both the film and the solid, indicating that the **A4** lanthanum film has the same in-plane metal phosphonate continuous lattice structure as the solid-state lanthanum phosphonates.[12] A similar comparison leads to analogous conclusions for the **A4**/Gd/**A4** film.

The orientation of the azobenzene chromophores in the films is determined through polarized IR studies.[55,57−59] The ratio of the absorbances of an IR mode measured with p-polarized light and s-polarized light can be related to the tilt angle that the transition dipole moment makes with respect to the surface normal. For the azobenzene chromophores, the tilt angles were evaluated over 2 or more bilayers in order to gain an improved signal-to-noise ratio. As a result, the calculated angles are averaged over both layers in a bilayer. The skeletal deformation mode 8a (1604 cm^{-1}, Figure 5B) that has its transition dipole moment

(53) Porter, M. D.; Bright, T. B.; Allara, D. L.; Chidsey, C. E. D. *J. Am. Chem. Soc.* **1987**, *109*, 3559−3568.
(54) Wood, K. A.; Snyder, R. G.; Strauss, H. L. *J. Chem. Phys.* **1989**, *91*, 5255−5267.
(55) Tillman, N.; Ulman, A.; Schildkraut, J. S.; Penner, T. L. *J. Am. Chem. Soc.* **1988**, *110*, 6136−6144.
(56) Frey, B. L.; Hanken, D. G.; Corn, R. M. *Langmuir* **1993**, *9*, 1815−1820.
(57) Haller, G. L.; Rice, R. W. *J. Phys. Chem.* **1970**, *74*, 4386-4393.
(58) Cammarata, V.; Atanasoska, L.; Miller, L. L.; Kolaskie, C. J.; Stallman, B. J. *Langmuir* **1992**, *8*, 876−886.
(59) Jang, W.-H.; Miller, J. D. *J. Phys. Chem.* **1995**, *99*, 10272−10279.

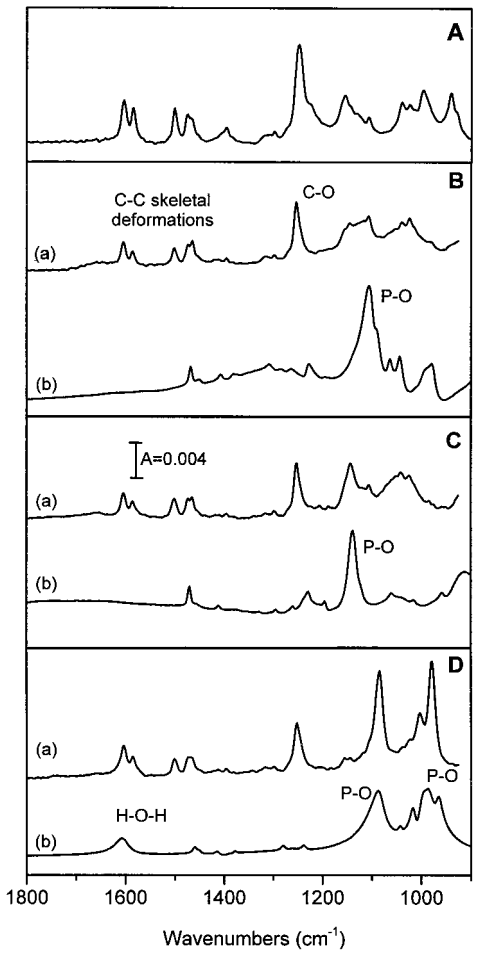

Figure 5. Comparison of the ATR-FTIR spectra of **A4** metal phosphonate LB films to those of KBr pellets of pure **A4** and solid-state layered phosphonates containing the same metal ion. (A) KBr pellet of **A4**; (B) (a) ATR-FTIR spectrum of one bilayer of an **A4**/La/**A4** film, (b) KBr pellet of lanthanum butylphosphonate; (C) (a) ATR-FTIR spectrum of one bilayer of an **A4**/Ba/**A4** film, (b) KBr pellet of barium decylphosphonate; (D) (a) ATR-FTIR spectrum of one bilayer of an **A4**/Mn/**A4** film, (b) KBr pellet of manganese ethylphosphonate. The absorbance scale in (C) refers to all of the LB films, and the KBr spectra in all cases are arbitrarily scaled for comparison. Band assignments are discussed in the text.

located along the C1−C4 axis of the aryl group was used.[55,60] The dichroic ratio leads to a tilt angle of 12 ± 2° for the azobenzene moiety in the **A4**/La/**A4** film, indicating a nearly perpendicular orientation in agreement with the optical spectroscopy results. Similarly, for the **A4**/Gd/**A4** film the IR analysis gives a chromophore tilt of 15 ± 2° from the surface normal.

Films with Structure Type $M(HO_3PR)_2$. The phosphonic acid **A4** easily transfers with barium, binding the metal in a 2:1 P:Ba ratio as predicted from the stoichiometry of solid-state barium organophosphonates (Table 2). XRD measurements yield an interlayer spacing of 66 Å (±2 Å), similar to the results obtained for the lanthanide films.

The optical absorbance spectrum of 5 bilayers of a barium **A4** film (Figure 2) is similar to that of the **A4**/La/**A4** film. As in the lanthanum film, the azobenzene groups are H-aggregated, evidenced by the blue shift of the $\pi-\pi^*$ transition to 298 nm. The relative intensities of the 298 and 250 nm bands also indicate that the long axes of the chromophores are upright with respect to the substrate. This orientation is confirmed with polarized IR experiments that give tilt angles of the azobenzene chromophores of 28 ± 2° in the barium film. Attempts to induce photochemical trans−cis isomerization led to no observable change in the optical spectrum.

To characterize the barium−phosphonate binding in the **A4**/Ba/**A4** film, the IR spectrum is compared to that of a KBr pellet of barium decylphosphonate in Figure 5C, where the significant P−O stretch is observed at 1143 cm^{-1}. Although the P−O stretches in the LB film are once again complicated by the presence of azobenzene-related bands, an intense P−O band also appears at 1143 cm^{-1}. The similarity in the energy of the stretches indicates that the in-plane structure in the film is the same as that in the solid-state sample.[12]

Films with Structure Type $M(O_3PR)\cdot H_2O$. Unlike the layered structure that Ba^{2+} adopts with monobasic phosphonates, divalent metals such as Mn^{2+} and Cd^{2+} form layered solids with formula $M(O_3PR)\cdot H_2O$. These different metal phosphonate structure types have also been observed in LB films formed from octadecylphosphonic acid.[10,12] However, in contrast to the barium−**A4** films described above, under our normal deposition conditions **A4** films with Mn^{2+} and Cd^{2+} form incompletely. At pH values where metal ions bind to the film, the extent of transfer is low, as evidenced by poor transfer ratios and low intensities in the optical and FTIR spectra. If the pH is lowered, **A4** transfer becomes facile, but FTIR analysis shows that no metal ions are incorporated into the film. As will be discussed in more detail below, it appears that there is a mismatch between the spacing of the aggregated azobenzene moieties on the water surface and the required phosphonate group spacing in the $M(O_3PR)\cdot H_2O$ layered solids. To transfer films of **A4** with the $M(O_3PR)\cdot H_2O$ structure, the aggregation that occurs in the Langmuir monolayer must be avoided.

Heating the subphase to 41 °C facilitates transfer of **A4** with manganese. At a subphase pH of 3.9−4.2, complete transfer of **A4** is achieved with complete manganese binding. The ATR-FTIR spectrum of the **A4**/Mn/**A4** film is shown in Figure 5D. The asymmetric and symmetric PO_3^{2-} stretches at 1087 and 979 cm^{-1} are well-defined and intense, just as they are for the manganese ethylphosphonate solid-state analogue whose spectrum is also shown in Figure 5D. There is an HOH bending mode near 1604 cm^{-1} in the ethylphosphonate spectrum, due to the coordinated water molecule that is overlapped by the C−C skeletal deformation mode 8a of the phenyl rings in the LB film spectrum. The HOH bend, coupled with a broad OH stretch at 3400 cm^{-1}, indicates that coordinated water is included in the LB film as it is in the solid-state manganese phosphonate analogue.[10,61] In contrast, water is not observed in LB films based on the other metal phosphonate structure types where lattice water is not present. The absorbance intensity of the C−C skeletal

(60) Varsanyi, G. *Vibrational Spectra of Benzene Derivatives*; Academic: New York, 1969.

(61) Nakamoto, K. *Infrared and Raman Spectra of Inorganic and Coordination Compounds*, 3rd ed.; John Wiley & Sons: New York, 1978.

deformations in one bilayer of the **A4**/Mn/**A4** film is the same as that in one bilayer of the **A4**/La/**A4** film, consistent with complete film transfer.

In Figure 2 the optical spectrum of 5 bilayers of the **A4**/Mn/**A4** film is shown, where the chromophores absorb with essentially the same intensity as in the **A4**/La/**A4** film, once again verifying complete transfer of the manganese **A4** phosphonate film at elevated temperatures. The $\pi-\pi^*$ transition is observed at 300 nm in the **A4**/Mn/**A4** film due to H-aggregated azobenzenes in the bilayers. XRD measurements on a 10 bilayer sample confirm the layered nature of the manganese LB film, affording an interlayer spacing of 64 Å (±2 Å), while XPS analysis establishes a 1:1 P:Mn ratio in the films, in agreement with the stoichiometry of the solid-state materials (Table 2).

Films with Structure Type $M(O_3PR)_2$. LB films of **A4** with Zr^{4+} can be deposited in a facile manner with the three-step deposition procedure described above. These films differ from those of the divalent and trivalent metals because the method for depositing the zirconium films results in an amorphous zirconium phosphonate layer rather than a crystalline network. XPS determination of the Zr:P ratio (Table 2) was performed at two stages of the deposition process, after zirconium binding to the template layer (step 2) and after completion of the bilayer. Within experimental error (±5%) the Zr:P ratio in the zirconated template is 1:1 indicating that one zirconium ion binds each phosphonate group in the template monolayer. Analysis of the **A4**/Zr/**A4** bilayer yields a 1:2 Zr:P ratio, confirming the complete transfer of the bilayer. This stoichiometry is consistent with the Zr:P ratios and ionic charges present in solid-state zirconium organophosphonates and is consistent with results seen for other zirconium phosphonate LB films.[1,7,8,11]

In the optical spectrum of 5 bilayers of an **A4** zirconium phosphonate film, seen in Figure 2, the λ_{max} of the $\pi-\pi^*$ transition can be found at 304 nm, a blue shift of 50 nm from the solution spectrum, indicating that the azobenzene units in the zirconium phosphonate films pack as H-aggregates as well. Once again the chromophores are aligned nearly upright, and polarized IR studies indicate a tilt from the surface normal of 26 ± 2° for the long axis of the azobenzene moiety. XRD yields an interlayer spacing of 63 Å (±2 Å), consistent with a nearly upright arrangement of the azobenzene chromophores in the film and similar to values obtained for other **A4** LB films.

The shoulder present on the low-energy side of the 304 nm band, attributed to nonaggregated chromophores, is very pronounced in this film, indicating a high percentage of areas containing isolated monomer or dimer units in the zirconium films. Irradiation of the $\pi-\pi^*$ transition with UV light to effect a trans−cis isomerization produces an observable change in the optical spectrum. As can be seen in Figure 1, the primary changes occurring after isomerization are a decrease in the intensity of the shoulder (near 355 nm) and an increase in the $n-\pi^*$ transition near 450 nm. The intensity changes are small but more pronounced than for the other **A4** metal phosphonate films. Assuming that the photochemical isomerization can take place in the defect areas of the film, there appears to be a slightly higher percentage of nonaggregated areas in the zirconium **A4** films than in the other examples. This observation is consistent with the deposition process used for the zirconium films, which is not expected to yield a crystalline metal phosphonate layer. The isomerization is reversible with visible light as well as with temperature.

Discussion

Characterization of each of the systems shows that **A4** forms stable, organized LB films with a variety of metal ions. In the hydrophilic region of the mixed organic/inorganic LB films, the metal phosphonates condense into known two-dimensional continuous lattice structures. The six metal ions studied here organize in four different metal phosphonate structure types. In the organic part of the film, the azobenzene chromophores pack as H-aggregates in each case, and only subtle differences are observed in the packing of the organic groups from one structure type to another. There is significant stabilization energy associated with the layered structures of both the organic and inorganic networks in these films. We now turn the discussion to how the preferred organization of the separate organic and inorganic components influence both the deposition of the films and the overall structure of the deposited films.

When the metal phosphonate LB bilayers are formed, the metal−headgroup interaction results in the crystallization of a two-dimensional continuous lattice. This process has been previously characterized for many octadecylphosphonate LB systems and is demonstrated here for several **A4** LB films. The inorganic continuous lattice component of the film is rigid, and for a given metal ion and structure type, the required spacing of the phosphonate headgroups is quite specific. Since the metal phosphonate layers are isostructural with their solid-state analogues, we can use known crystal structures to determine what the phosphonate spacings need to be to form each metal phosphonate lattice. Inspection of the crystal structures reveals that the phosphonate spacing differs from one structure type to the next. These different spacing requirements necessitate appropriately tuned deposition conditions to form the different metal phosphonate LB layers.

The phosphonate spacing in each structure type can be obtained from the series of metal phenylphosphonates $Mn(O_3PC_6H_5)\cdot H_2O$, $Ba(HO_3PC_6H_5)_2$, and $LaH(O_3PC_6H_5)_2$ for which the crystal structures have been published.[16,18,21] Since these structures are layered, the phosphonate spacings within each layer can be expressed in terms of the "area per phosphonate group", allowing for direct comparison to the molecular spacings in the LB films. The "area per phosphonate group" in the lanthanum and barium phenylphosphonates is 21 and 23 $Å^2$, respectively, while in manganese phenylphosphonate the value is close to 28 $Å^2$. The similar values for the lanthanum and barium salts reflect the 1:2 metal:phosphonate stoichiometry for each, while the "area per phosphonate group" is larger in the manganese salt due to the 1:1 stoichiometry. These phosphonate spacings can now be compared to the packing of the azobenzene chromophores.

Through optical spectroscopy we have demonstrated that the azobenzene groups are strongly H-aggregated

in each of the metal phosphonate films of **A4**. LB films containing azobenzene chromophores have been widely studied, and H-aggregation is commonly observed. Recently, Whitten and co-workers used Monte Carlo cooling methods to analyze the packing of azobenzene-derivatized fatty acids in LB films.[25] The optimized packing, consistent with the observed optical spectroscopy, presents the azobenzene units in a herringbone array that is much like the solid-state packing in the crystal structure of azobenzene itself.[62] From this model, the calculated "area per molecule" of the azobenzene chromophores is approximately 22 Å^2. The preferred "area per molecule" of the aggregated azobenzene groups is very close to the "area per phosphonate group" required to form the $LaH(O_3PR)_2$ and $Ba(HO_3PR)_2$ metal phosphonate structures. Indeed **A4** films with La^{3+} and Ba^{2+} form quite easily at room temperature, and the H-aggregation in the transferred films is consistent with the spacing requirements of the metal phosphonate continuous lattice structure.

In contrast there is a large mismatch in the preferred spacings of the azobenzene chromophores and the "area per phosphonate group" in the manganese (or cadmium) phosphonate structures. This mismatch affects both the deposition process and the structure of the transferred films. Azobenzene amphiphiles are known to aggregate on the water surface, and the room-temperature pressure vs area isotherm of **A4** on a water subphase (Figure 6A) suggests the molecules are already aggregated. The surface pressure rises abruptly at 27 Å^2/molecule, and there is a well-defined liquid condensed region between 25 and 27 Å^2/molecule. To achieve the spacing required (28 Å^2) to form the $M(O_3PR)\cdot H_2O$ structure with either Cd^{2+} or Mn^{2+}, the aggregates need to break-up. At room temperature the aggregates are well-established, and film transfer with Cd^{2+} or Mn^{2+} is inefficient. Even though formation of the metal phosphonate continuous lattice should provide a substantial benefit in lattice energy, the aggregation of the **A4** amphiphiles at the air/water interface provides a kinetic barrier to the deposition.

The barrier to deposition is overcome by thermally breaking-up the aggregates. The temperature dependence of the aggregation is reflected in the pressure vs area isotherms of **A4** measured on a 0.5 mM Mn^{2+} subphase at 24 and 41 °C (Figure 6B). For comparison, isotherms of OPA on a water subphase at room temperature and at 41°C are included in Figure 6A. For OPA the isotherms are similar at the two temperatures except for the lower collapse pressure at higher temperature. However, in the case of **A4**, not only does the collapse pressure decrease at 41 °C but, in addition, the slope becomes flatter and the whole isotherm shifts to higher mean molecular area. These changes in the isotherm indicate a significant decrease in the extent of **A4** aggregation at higher temperatures. Under these conditions, transfer of **A4** with Mn^{2+} and Cd^{2+} becomes facile. Transfer ratios and spectroscopic analyses of the transferred films are consistent with complete transfer of **A4** and formation of the $M(O_3PR)\cdot H_2O$ metal phosphonate structure type.

After the film is transferred, the azobenzene chromophores appear to reorganize. The $\pi-\pi^*$ transition

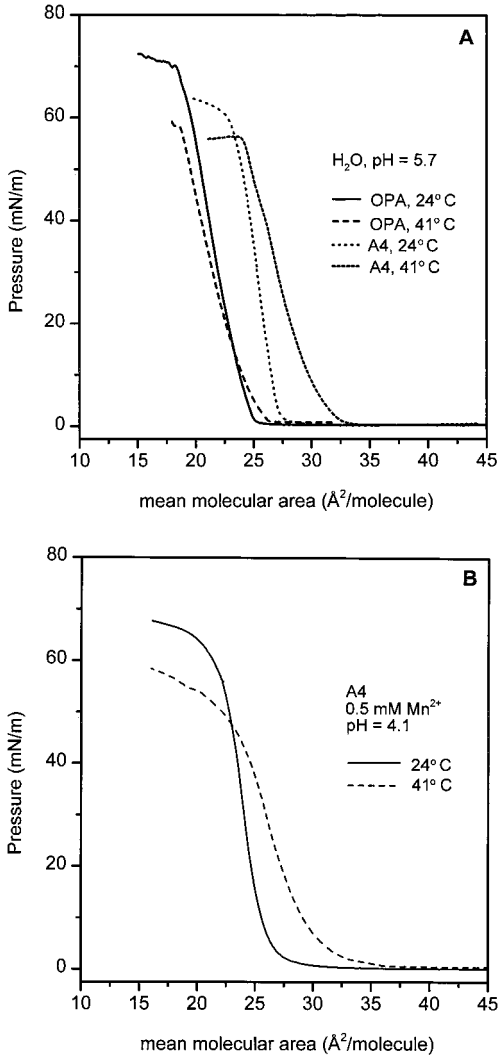

Figure 6. Pressure vs mean molecular area isotherms as a function of temperature: (A) OPA and **A4** on a water subphase (pH 5.7, unadjusted) at 24 and 41 °C; (B) **A4** on a manganese subphase (pH 4.1) at 24 and 41 °C. Spreading solutions used in the experiments had concentrations of 1.1 mg/mL in 10% EtOH/$CHCl_3$ for OPA and 0.2–0.3 mg/mL in 15% EtOH/$CHCl_3$ for **A4**. Isotherms were performed with a linear compression rate of 8 mN/(m/min) and with maximum barrier speeds of 10 mm/min.

in the **A4**/Mn/**A4** film is observed at 300 nm, indicating that the azobenzene groups have re-formed the close-packed H-aggregates despite the spacing requirements imposed by the rigid manganese phosphonate inorganic lattice. To achieve both H-aggregation of the azobenzene chromophores and formation of the $M(O_3PR)\cdot H_2O$ metal phosphonate structure type suggests that the spacings within the organic and inorganic networks are incommensurate. The incommensurate packing is possible because of the flexible four-carbon alkyl tails linking the azobenzene groups and the phosphonate headgroups. In this scenario, domains of azobenzene aggregates are attached to the inorganic lattice by the alkyl linkers which compensate for the mismatched lattice spacing through disorder in the four-carbon chains. Evidence for this disorder appears in the FTIR, where there is a shoulder on the high energy side of the 2918 cm^{-1} $\nu_a(CH_2)$ band, similar to that in the La^{3+} film shown in Figure 4.

(62) Brown, C. J. *Acta Crystallogr.* **1966**, *21*, 146–152.

The incommensurate packing of the organic and inorganic networks has a parallel in a recent study by Caldwell et al. on the adsorption of alkylthiol-derivatized azobenzene chromophores onto a Au(111) surface.[63] In-plane XRD and AFM studies indicated that the azobenzene aggregation was incommensurate with the underlying Au(111) surface. The authors proposed a model where the azobenzene units pack in a herringbone fashion to form bundles of ordered azobenzene groups (~80 units/bundle) where the aggregates are tethered to the surface by the flexible alkylthiol chains which adsorb in the usual ($\sqrt{3} \times \sqrt{3}$)R30° pattern on the Au surface. A similar picture can be envisioned for the **A4**/Mn/**A4** LB films (and to a lesser extent the **A4**/La/**A4** and **A4**/Ba/**A4** films as well). As the films form, the inorganic lattice crystallizes. The ionic/covalent inorganic network contributes a major portion to the overall lattice energy of the organic/inorganic assembly. The next largest energy component is the π-stacking of the azobenzene chromophores, and they will seek to maximize their stabilization, aggregating within the constraints imposed by the inorganic network. In the **A4** films, the four-carbon tether provides the flexibility necessary to allow the azobenzene groups to form the same H-aggregates they would in the absence of the metal phosphonate network. The final component of the assembly is the 14-carbon alkyl tail which then tilts, if necessary, to maximize van der Waals contacts. The C−H stretching modes in the FTIR demonstrate that the 14-carbon alkyl tails are close-packed and all-trans.

The zirconium phosphonate film can be considered differently because of the discrete three-step deposition procedure that is used. The deposition process still relies on the affinity of the zirconium ions for the phosphonate ligands, but unlike the examples with the divalent and trivalent metal phosphonates, the zirconium phosphonate network is largely amorphous. Although not demonstrated here for the **A4** films, previous work has shown that the three-step deposition procedure can result in bilayers where the organization in the template layer differs from that in the capping layer.[11] The zirconium phosphonate films are attractive because they are stable in nearly any organic or aqueous media.[8]

Summary

This study demonstrates that the metal phosphonate approach of forming continuous lattice LB films, previously developed for alkylphosphonates, can be extended to functional phosphonic acid derivatives. LB films of **A4** with divalent, trivalent, and tetravalent metal ions have been prepared where the inorganic lattice possesses the same metal phosphonate bonding that these metal ions exhibit in solid-state metal phosphonate phases. In each of the deposited films, the azobenzene units H-aggregate and are oriented nearly parallel to the substrate normal. Isomerization experiments produce no observable change in the optical spectrum for the divalent and trivalent metal films, and it is only in the zirconium films that the characteristic cis peak appears upon irradiation at 365 nm.

Film deposition in each case depends on the preferred packing of the inorganic and organic components of the films. For films prepared with barium or lanthanide ions, transfer is facile because the preferred spacing of the organic groups is nearly commensurate with the inorganic lattice parameters. However, the large mismatch between the preferred "area per molecules" of the H-aggregated azobenzene groups and the phosphonate headgroups in the manganese and cadmium films hinders complete film transfer. Here the kinetic barrier to film reorganization on the water surface is too large and deposition can only be achieved at elevated temperatures. Subphase temperatures of 41 °C provide sufficient thermal energy to break-up the aggregation on the water surface, allowing for the phosphonate spacing on the surface to match that in the manganese and cadmium layered phosphonates, thereby encouraging film transfer. Upon transfer, the azobenzene units once again aggregate to maximize their overlap in the films. In the case of the zirconium films, the organic and inorganic lattices do not need to be commensurate for film transfer because the stepwise nature of the deposition procedure allows the organic and inorganic networks to form independently of one another.

Acknowledgment. We are grateful to the National Science Foundation for financial support. M.A.P. thanks the National Science Foundation for a predoctoral fellowship. We thank Professor Kirk Schanze and Mr. Kevin Ley for assistance with the photochemical isomerizations and the experimental setup. Special thanks are extended to the University of Florida Major Analytical Instrumentation Center for use of the XRD and XPS facilities.

CM980406Z

(63) Caldwell, W. B.; Campbell, D. J.; Chen, K.; Herr, B. R.; Mirkin, C. A.; Malik, A.; Durbin, M. K.; Dutta, P.; Huang, K. G. *J. Am. Chem. Soc.* **1995**, *117*, 6071−6082.